CHAPTER 4

Sagwan sawdust pyrolysis and Product characterizations

4.1 Introduction

According to the statistics provided by the United Nations, the population of the world was 7.2 billion in the year 2013 and it is expected to increase by 33% in the year 2050 (Tripathi et al., 2016). With this increase in population, demand in every aspect (food, shelter, energy, etc.) is becoming higher continuously. In the present scenario, around 90% of the energy consumption in developing countries is fulfilled by fossil fuels (Azar et al., 2003). These conventional resources are for a limited period of time and continuous usage produces harmful gases responsible for global warming (Sharma et al., 2015). Therefore, there is a need for renewable, sustainable, cost-effective and alternative source of energy. Among the available resources, biomass is easily available largest and most sustainable energy resource (Zhang, 2010) and it contributes around 14% of world energy consumptions (Balat and Ayar, 2005). Other advantages of biomass include carbon dioxide neutral and low sulphur and nitrogen content (Mahinpey et al., 2009) resulting in less SO_x and NO_x emission as compared to fossil fuels.

Among various thermochemical methods (combustion, gasification, pyrolysis and liquefaction), pyrolysis is most promising and eco-friendly technique (Mohan et al., 2006) to degrade biomass into various products (bio-oil, biochar and pyrolytic gas) in an inert atmosphere and to get higher HHV fuels. Product distribution in pyrolysis process depends upon various factors like temperature, heating rate, packed bed height, residence time, reactor type, etc. Bio-oil is a complex liquid mixture of high water content and oxygenated organic compounds (Zhang et al., 2017). Acidity and chemical instability of bio-oil makes it unsuitable for direct use. It requires upgrading processes to enhance its HHV, for its direct use in industries. However, it contains valuable chemicals which can be a source of feedstock for many industries.

In addition to bio-oil, biochar is also a solid value-added product obtained from pyrolysis. According to the definition given by International Biochar Initiative (Lehman and Joseph, 2015), biochar is a carbon-rich stable solid material obtained after thermochemical conversion of biomass in oxygen limited environment and its properties depend upon various operating process parameters. Various applications of biochar include waste management as it decreases the volume of waste, energy requirement for its transport and also reduces methane emission when land filled (Kwapinski et al., 2010; Hossain et al., 2011), solid fuel (Zhang et al., 2017), high efficient low cost adsorbent for air and water pollutant (Mohan et al., 2011), catalyst (Lee et al., 2017), upgrading to activated carbon (Ahiduzzaman and Sardul Islam, 2016) and in soil amendment (Cha et al., 2016).

Non-condensable gases are the other useful byproducts obtained during pyrolysis. These non-condensable fractions are the mixture of useful gases such as hydrogen, methane, carbon monoxide, etc. which has high calorific value and they have their utility in the field of power generation.

SS is a lignocellulosic waste biomass which is not easily biodegradable and creates disposal problem. Thus valorization of this forestry waste for biofuel production is both sustainable and economically profitable. Details regarding production and utilization of SS are discussed in section 3.1.

In previous studies, Ismadji et al. (2005) performed the vacuum pyrolysis of SS for the preparation of activated carbon with very high BET surface area. Balogun et al. (2014) studied the devolatilisation kinetics and pyrolysis of Nigerian sawdust using iso-conversional methods and the bio-oil collected at 500 °C confirmed the presence of various valuable chemical compounds. Pyrolysis of SS at 450 °C was performed by Bardalai and Mahanta, (2018) to investigate the physico-chemical properties of bio-oil for its application in engines.

From the aforesaid facts, the study was designed to convert the SS into useful products in an energy efficient manner using pyrolysis. Prior to experiments, initial characterizations were done to find the suitability of SS for pyrolysis. The effect of operating parameters like temperature, sweeping gas flow rate, packed bed height and particle sizes were investigated to see their impact on the yield of valuable products (biochar, bio-oil and pyrolytic gas). Further, characterizations of products were done to find their possible use in various fields. This work was organized for the pyrolysis of SS by varying the process parameters and in-depth characterization of all the products obtained.

4.2 Experimental

4.2.1 Raw material

SS collection and its initial treatment have been discussed in section 3.2.1. After drying, SS was sieved with mesh (25, 36, 60 and 80) to get different particle sizes of desired range. Mesh size of -25+36, -36+60 and -60+80 represents particle size 0.42-0.60, 0.25-

0.42 and 0.18-0.25 mm, respectively. Prepared samples were then collected in sample containers and were kept in desiccators at room temperature for further experiment.

4.2.2 Chemicals and reagent

All the reagents and chemicals used for the research work were of analytical grade and the solutions were prepared with DDW. The chemicals used for pyrolytic gas cleaning were dichloromethane (CH_2Cl_2) 99 %, silica gel and acetone 99 %.

4.2.3 Pyrolysis experimental procedure

The pyrolysis experiments were performed in a vertical tubular packed bed reactor made up of stainless steel of length 500 mm and inner diameter of 42 mm in which temperature was maintained using proportional-integral-derivative (PID) controller. A schematic diagram of experimental set-up is given in Fig. 4.1. 20 g of oven dried biomass sample was fed to the reactor and then reactor was properly sealed with gasket to prevent any leakage of products to the atmosphere. An electric Narang Scientific Works (NSW)-104 split tube furnace single zone was used for the pyrolysis experiments. Nitrogen gas was purged continuously inside the reactor at the flow rate of 150 mL/min to make sure that there was no oxygen inside the reactor and also to maintain inert atmosphere inside the reactor. The thermal pyrolysis experiments were performed in the temperature range of 400 – 700 °C in 100 °C intervals, respectively. The reactor was maintained at its final temperature for 60 min to ensure proper reactions to occur. Reactor outlet was connected to the conical flask joined in series with two others and were dipped in ice cooled condenser system where condensable hydrocarbon vapours were condensed and non-condensable gases were collected in the sample containers after passing it through dichloromethane and silica gel column for the removal of MC and solid impurities. In next group of experiments to see the effect of nitrogen flow rate, 20 g of SS was pyrolysed at a fixed temperature of 600 °C and

particle size of 0.18-0.25 mm with nitrogen flow rates of 150, 200 and 250 mL/min. For the effect of packed bed height, it was varied from 2-8 cm keeping temperature, particle size and nitrogen flow rate fixed at 600 °C, 0.18-0.25 mm and 150 mL/min, respectively. For the effect of particle size, 20 g of SS in the size range of 0.42-0.60, 0.25-0.42 and 0.18-0.25 mm were used for the pyrolysis experiments at temperature 600 °C and sweeping gas flow rate of 150 ml/min. The biochar from the process was the left over solid residue inside the reactor which was collected after cooling the system. Bio-oil was the liquid collected in the conical flasks connected in series after condensation. Produced bio-oil was centrifuged and separated from water by decantation using separating funnel and was taken for analysis. The pyrolytic gas was stored in the gas bags. The yield of products after pyrolysis process was calculated by the equations described below.

$$\textbf{Biochar yield (\%)} = \left(\frac{\textbf{Weight of biochar}}{\textbf{Weight of total feed}}\right) \times \textbf{100} \quad \textbf{(4.1)}$$

$$\textbf{Bio-oil yield (\%)} = \left(\frac{\textbf{Weight of bio-oil}}{\textbf{Weight of total feed}}\right) \times \textbf{100} \quad \textbf{(4.2)}$$

$$\textbf{Gas yield (\%) = 100 – (biochar yield + bio-oil yield)} \quad \textbf{(4.3)}$$

All the experiments were performed in triplicate and average value has been reported. Produced biochar and bio-oil were named as BC and BO followed by the temperature at which they were produced (e.g. BC 400 indicates biochar produced at 400 °C).

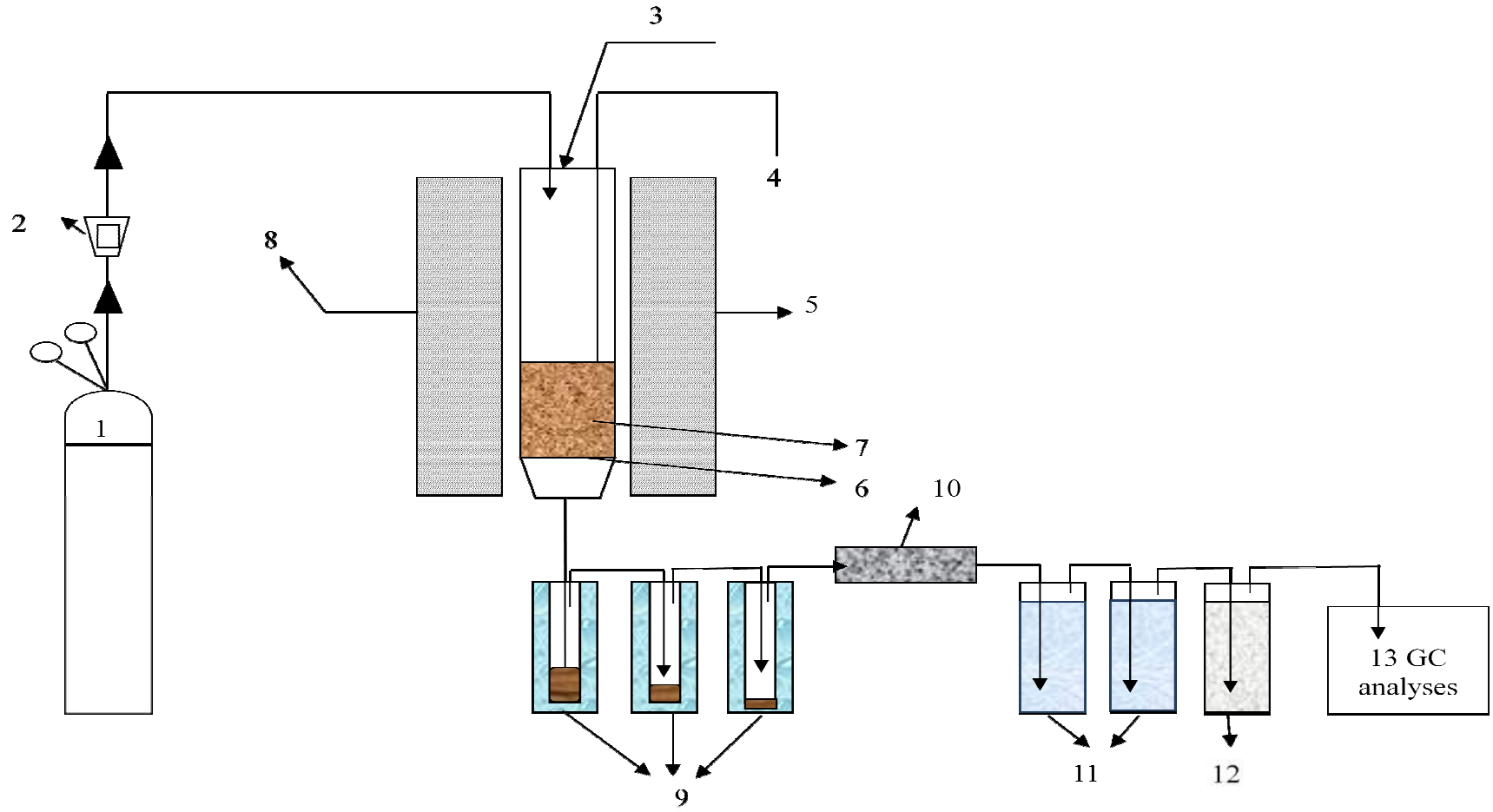

Fig. 4.1 Schematic diagram of experimental set-up: 1.Nitrogen cylinder 2.Rotameter 3.Stainless steel reactor 4.Thermo couple 5.Electric furnace 6.Perforated support 7.Biomass sample 8.Electric power supply 9.Ice bath chiller 10.Cotton filter 11. Dichloromethane 12.Silica gel column 13.Gas collector

4.2.4 Analytical methods and instruments used for product characterizations

4.2.4.1 Biochar characterization techniques

Proximate analysis of biochar was done according to standard ASTM methods. MC, AC and VM of the samples were measured using standard method of ASTM D3173, ASTM D3174 and ASTM D3175, respectively. FC was calculated by difference according to equation 4.4:

$$FC = [100 - (MC+AC+VM)] \% \quad (4.4)$$

Ultimate analysis and HHV for biochar were determined in similar way as discussed in section 3.2.2.

Energy yield (EY) of biochar was calculated from the equation shown below:

$$EY = \text{Yield of biochar} \times \left(\frac{HHV_{biochar}}{HHV_{biomass}}\right) \quad (4.5)$$

Fourier transforms infrared spectroscopy (FTIR) of SS and produced biochar was obtained for the identification of different functional groups using Thermo-Nicolet 5700 spectrophotometer (USA). Pellets were prepared using hydraulic press by mixing the sample with KBr in the ratio (sample: KBr) of 1:10 and were analyzed in the infrared region of 4000 – 400 cm^{-1} taking blank KBr pellet as reference.

X-ray diffraction of SS and biochar were recorded by Rigaku Mini Flex 600 operating at 40 kV and 15 mA using Cu Ka 1 radiation source of wavelength, k = 1.5405 Å in the 2Θ range of 5-70 º. The crystallinity index of the samples was calculated using the following equation 3.9:

$$\text{Crystallinity index} = \left(\frac{I_{002} - I_{am}}{I_{002}}\right) \times 100 \quad (4.6)$$

Where, I_{002} is the maximum intensity (in arbitrary units) of the 002 lattice diffraction and I_{am} is the intensity of diffraction in the same unit at 2Θ = 18° (Rojith and Singh, 2012).

The morphological changes on the surface and qualitative inorganic elemental composition of SS and its biochar were determined by scanning electron microscope ZEISS EVO 18 RESEARCH (Germany) outfitted with an energy dispersive X-ray spectrometer.

To get the Brunauer–Emmett–Teller (BET) surface area of the biochar, nitrogen adsorption - desorption isotherms were determined on an ASAP 2020 adsorption apparatus (Micromeritics, USA) at - 196 °C. The degassing of the sample was done at 300 °C using liquid nitrogen.

4.2.4.2 Bio-oil characterization

Physical and chemical characteristics of bio-oil produced after pyrolysis at different temperatures were analyzed for carbon residue, density, kinematic viscosity, HHV, pH, AC, functional groups and chemical constituents. Carbon residue was measured by Ramsbottom carbon residue apparatus (IP 14/65) (The National Scientific Instruments and Co., Delhi, India). Density of the bio-oil was measured according to the standard methods of ASTM D 1298. HHV of the bio-oil samples were measured using bomb calorimeter (IP 12/63T, Rajdhani Scientific Instruments Co. Delhi, India). The kinematic viscosity of the bio-oil was measured using Redwood viscometer (IP 70/46, GALLENKAMP, British made) and the pH of the bio-oil was determined using Systronics digital pH meter (Ahmedabad, India). AC for the bio-oil was determined following the standard method from ASTM D 482. FTIR analysis of the liquid samples was obtained by Thermo-Nicolet 5700 FTIR spectrophotometer (USA) in the wave number range of 4000–400 cm^{-1} for the identification of different functional groups.

The components present in the bio-oil were identified using VARIAN 240 GC–MS with VM5MS capillary column (30 m × 250 mm × 0.25 mm) in the continuous supply of helium as carrier gas. 1 µl of sample was injected into the column using a 1:10 split

ratio and injector temperature was set at 250 °C. At the start, oven temperature was 40 °C, held for 10 min, raised to 240 °C with ramping rate of 10 °C detained for 15 min and finally raised to 275 °C with the rate of 10 °C/min, held for 10 min. National Institute of Standards and Technology (NIST) library was used as reference for the identification of obtained chromatographic peaks.

4.2.4.3 Pyrolytic gas characterizaton techniques

The compositional analysis of the pyrolytic gas was performed by gas chromatography (GC) (NUCON 5765) using thermal conductivity detector (TCD) and flame ionization detector (FID). Stainless steel porapak-q column of dimension (2 m × 2 mm) was used for the detection purpose. Nitrogen at the flow rate of 25 mL/min was supplied as the carrier gas. The oven temperatures were set at 110 °C and 70 °C for TCD and FID, respectively. The injector and detector temperature for GC-TCD was 110 °C and 120 °C and for GC-FID it was 70 °C and 80 °C, respectively. 0.1 mL of gas sample was injected using Hamilton-Bonaduz-Schweiz gastight syringe for the quantitative analysis. All the experiments were performed in triplicate and average values were reported.

4.3 Results and Discussions

4.3.1 Physicochemical properties of SS

The physicochemical characteristics of SS are already discussed in section 3.3.1.

4.3.2 Effect of process parameters on the yield of pyrolysis products

4.3.2.1 Effect of temperature

Temperature plays an important role in the product distribution (bio-oil, biochar and pyrolytic gas) of pyrolysis process as depicted in Fig. 4.2. With the increase in temperature from 400 to 700 °C the biochar yield decreased from 37.42 to 26.45 wt. %. The decrease in the biochar yield could be due to greater primary degradation of biomass at higher temperature or due to occurrence of secondary cracking reactions

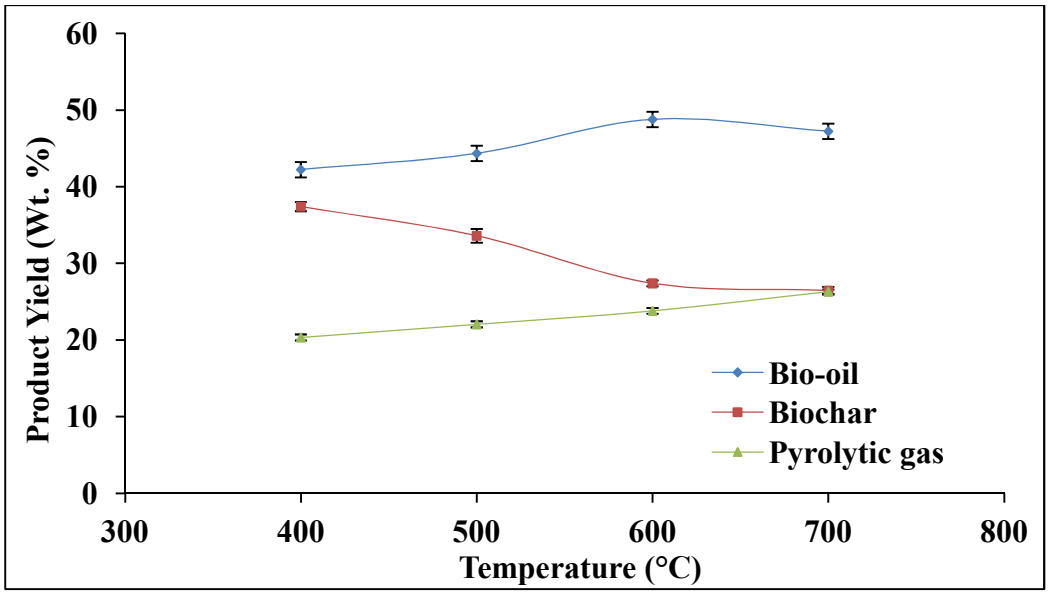

Fig. 4.2 Effect of temperature on yield of pyrolysis products

leading to decompositions of the char residues (Horne and Williams, 1996). Bio-oil yield increased from 42.24 wt. % at 400 °C to 48.8 wt. % at 600 °C, and then it decreased to 47.25 wt. % at 700 °C. This temperature was adequate for the complete pyrolysis reaction to take place and simultaneously this temperature was not sufficiently high for the occurrence of secondary reactions (Kader et al., 2013) and so, maximum liquid yield was observed. Thus, 600 °C was chosen as the optimum temperature for the pyrolysis process. The pyrolytic gas yield increased from 20.34 to 26.3 wt. % with increase in temperature. Increase in the bio-oil yield is reasonable as more and more VM are removed with rise in temperature but at higher pyrolysis temperature secondary cracking reactions of volatile compounds occur that results in more non-condensable gases which contribute to lower bio-oil and biochar yield (Choudhury et al., 2014). Similar result was observed by Rout et al., (2016) for coconut shell pyrolysis.

4.3.2.2 Effect of sweeping gas flow rate

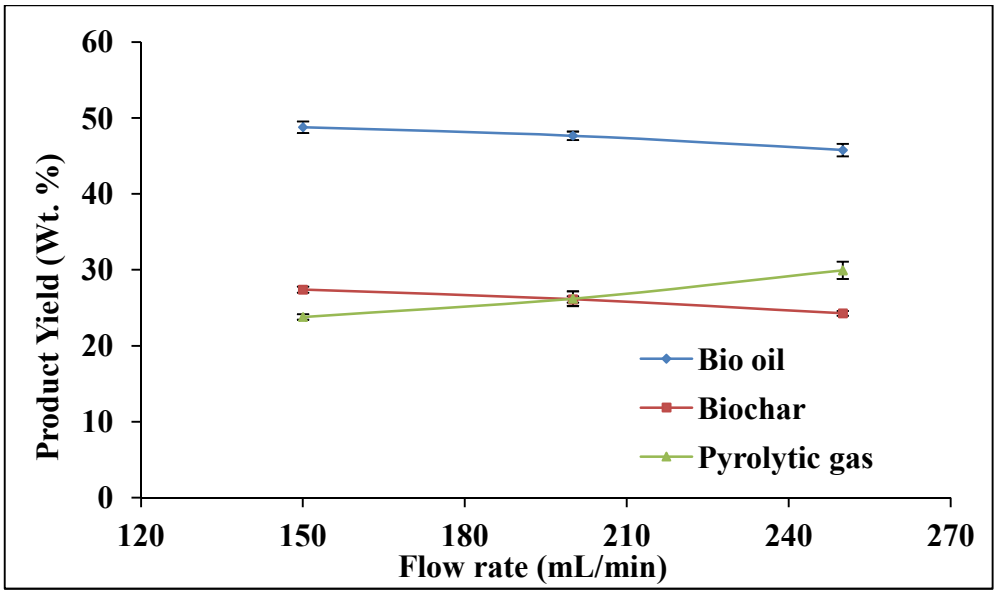

Fig. 4.3 Effect of sweeping gas flow rate on yield of pyrolysis products

Effect of sweeping gas (N_2) flow rate on pyrolysis product yield is presented in Fig. 4.3. With the increase in flow rate of sweeping gas there was slight decrease in bio-oil and biochar yield. Bio-oil yield decreased to 45.78 from 48.80 wt. % and biochar yield decreased to 24.27 from 27.40 wt. %. Increase in sweeping gas flow rates reduced the vapour residence time inside the reactor and pushed the vapours out of the reaction zone which stops the secondary reactions like thermal cracking, repolymerization and recondensation (Demiral et al., 2012). In addition, higher flow rate also decreased the vapour residence time inside the condenser and some part of the condensable fraction was also escaped along with non-condensable fractions as gaseous product. Thus pyrolytic gas yield increased from 23.80 to 29.95 wt. % as the sweeping gas flow rate increased from 150 to 250 mL/min.

4.3.2.3 Effect of packed bed height

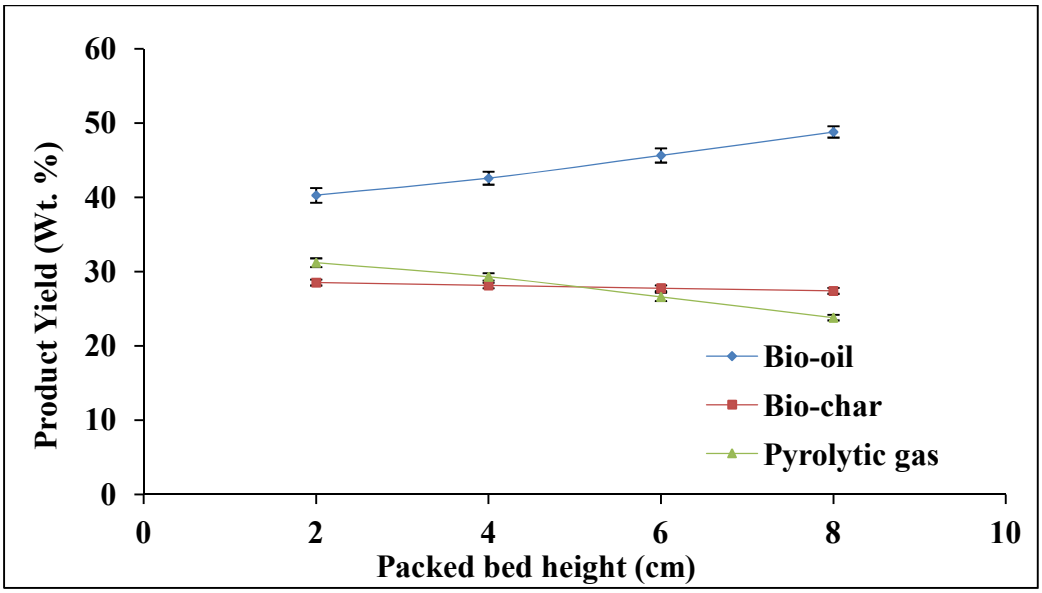

Fig. 4.4 Effect of packed bed height on yield of pyrolysis products

Effect of packed bed height on pyrolysis product yield is very less studied parameter previously but it also affects the product distribution severely. The bed height variations were done from 2 to 8 cm keeping biomass bed at the centre of heating zone. Increase in the packed bed height from to 2 to 8 cm showed an increase in bio-oil yield from 40.27 to 48.80 wt. % and very slight decrease in biochar yield from 28.53 to 27.40 wt. % and pyrolytic gas yield from 31.20 to 23.80 wt. % as shown in Fig. 4.4. This could be due to increase in the packed bed height resulted in a longer residence time in the dense biomass bed and more secondary cracking reaction which subsequently caused the primary organic vapours to crack and form more volatile product and less biochar yield. Similar result was observed by Zhang et al. (2009) who reported that with an increase in the static bed height from 5 to 10 cm, the bio-oil yield increased while biochar and gas yield decreased.

4.3.2.4 Effect of particle size

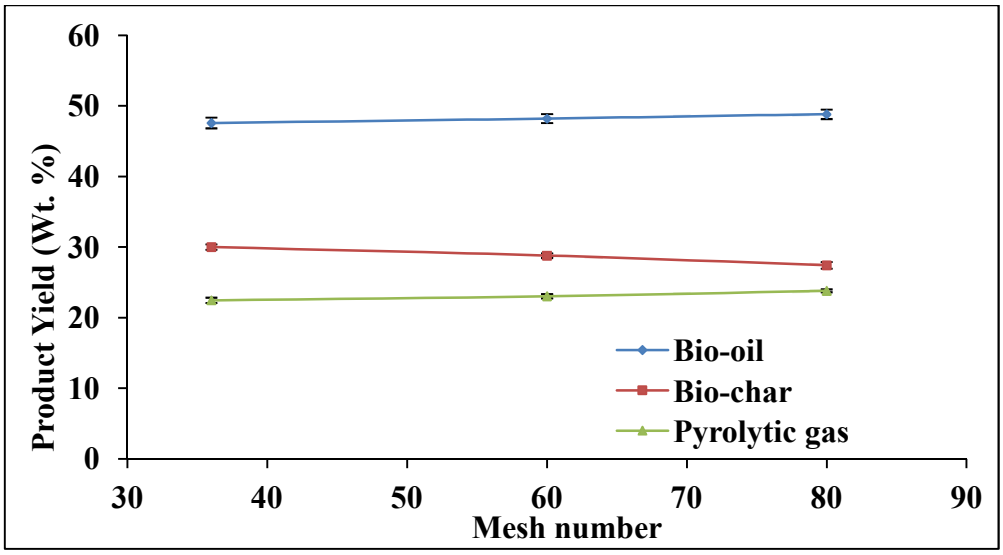

Fig. 4.5 Effect of particle size on yield of pyrolysis products

Particle size has not such major effect on product yield in the present study. With the increase in particle size biochar yield was increased while bio-oil and pyrolytic gas showed a reverse profile as shown in Fig. 4.5. This could be because in a larger particle size, heating rate is slower to the particle interior and vapours coming out have to travel longer distance. This causes longer residence for the vapour to come out and secondary reactions occur leading to higher char yield (Zhang et al., 2009). Similar result was observed by Shen et al. (2009) for oil mallee woody biomass where bio-oil yield decreased with increase in particle size.

4.3.3 Characterization of biochar

4.3.3.1 Physico-chemical characterization

To measure the quality of biochar as effective solid fuel, proximate analysis, ultimate analysis and HHV of biochar was done and the results are presented in Table 4.1.

Proximate analysis of biochar samples illustrates that, with increase in temperature from 400 to 700 ˚C, VM showed a decreasing trend from 25.61 to 9.37 wt. %, in parallel FC increased from 64.22 to 76.68 wt. %. AC also increased from 7.5 to 12.22 wt. % with rise in temperature. This is mainly due to the removal of volatiles present in feedstock and accumulation of inorganic elements present (Tag et al., 2016). Although the amount of AC in biochar is higher in comparison to parent biomass but it is much lower as compared to Indian fossil coal with AC in the range of 25 to 40 wt. % (Anupam et al., 2016). High AC is not desirable as it brings down the energy value of the fuel. The ratio of VM/(VM + FC) in the biochar decreased by 87.08 wt. % for the final biochar. Reduction in this ratio along with increase in FC symbolizes better fuel qualities (higher HHV) of biochar in comparison to SS.

Elemental analysis of biochar samples showed increased carbon content with rise in temperature but oxygen and hydrogen content showed reverse profile which is due to increasing degree of carbonization (Al-Wabel et al., 2013). Reduced oxygen content and higher carbon content stands for better fuel properties (higher HHV) of biochar (Sheng and Azevedo, 2005). The atomic ratios O/ C, H/C and (N + O)/C of feedstock and biochar revealed that, SS has highest of these ratios and which tend to decrease with rise in temperature from 400 to 700 °C. Increase in temperature is associated with dehydration reaction and thus O/C ratio is decreasing and making biochar more hydrophobic i.e. less hydrophilic (Gupta et al., 2018). Decrease in H/C ratio is indicative of higher degree of carbonization and increasing fuel value (HHV). Decreasing nature of (N + O)/C explains the aromaticity and decrease in polarity of biochar.

Table 4.1 Proximate, ultimate, HHV and EY analysis of biochar

	BC 400	BC 500	BC 600	BC 700
Proximate analysis (wt. %)				
MC	2.67	2.12	1.97	1.73
VM	25.61	17.88	12.87	9.37
FC*	64.22	69.11	73.33	76.68
AC	7.50	10.89	11.83	12.22
VM/(VM+FC)	0.285	0.206	0.149	0.109
Ultimate analysis (wt. %)				
C	71.69	75.51	78.97	81.59
H	3.98	3.17	2.48	2.12
N	1.17	1.23	1.29	1.37
O*	23.17	20.09	17.26	14.92
S	bdr	bdr	bdr	Bdr
Atomic ratios				
H/C	0.66	0.50	0.37	0.31
O/C	0.24	0.20	0.16	0.14
(N+O)/C	0.25	0.21	0.17	0.15
HHV (MJ/kg)	27.17	27.51	28.19	28.93
EY	0.573	0.521	0.436	0.432

bdr - indicates below detection range, * by difference

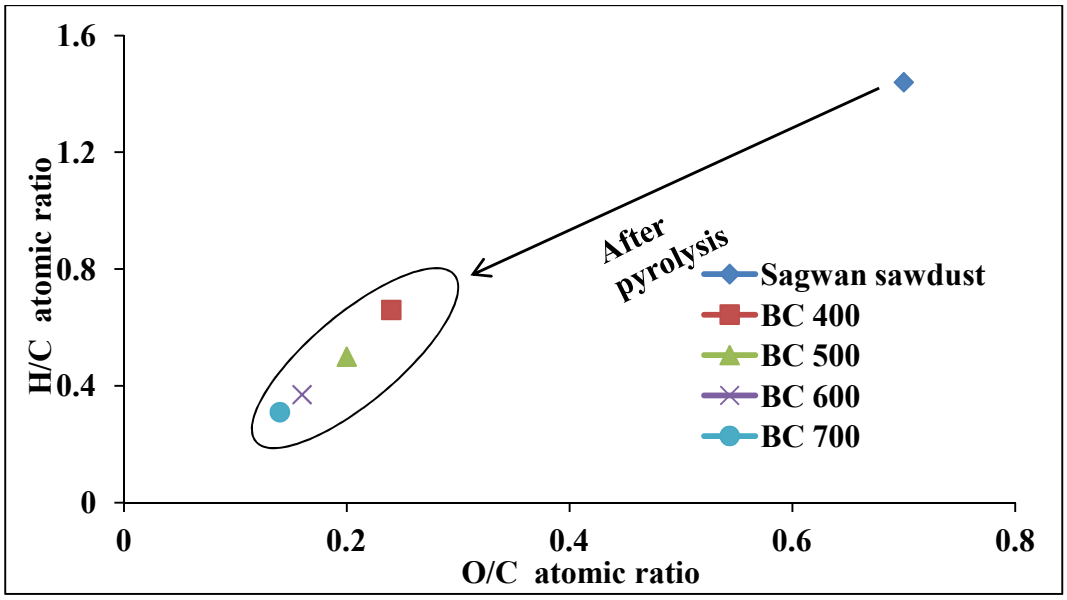

Fig. 4.6 Van Krevelen diagram for SS and its biochar

The Van Krevelen diagram of SS and biochar is shown in Fig. 4.6. SS has the location like other biomass samples (Senneca, 2007) but biochar shifts towards lower value and at higher temperatures i.e. 600 and 700 °C, they lie in the region of anthracite. Similar type of result was obtained by Varol et al. (2007) for pistachio shell pyrolysis. Lower value of these ratios is attractive as they account for lower energy loss, smoke and water vapour during combustion (Zhang et al., 2017a, b; Anupam et al., 2016).

Increase in FC and decrease in oxygen content led to increase in the HHV of the biochar i.e. from 17.86 MJ/kg of SS to 28.93 MJ/kg of BC 700. The HHV of biochar produced from SS was higher as compared to biochar prepared from vine pruning, poultry litter, orange pomace and seaweed (Tag et al., 2016). These higher HHV of biochar show its utility as solid fuel.

Energy yield represents the amount of remaining energy in the pyrolysis products from the product yields and their HHV values (Chen et al., 2015). The energy yield for the biochar at different temperatures is reported in Table 4.1. Increase in pyrolysis

temperature led to the decrease in energy yield of biochar and maximum decrease was at higher temperature. This is because at higher temperature more volatiles were converted to liquid and gaseous products and the energy was shifted towards liquid and gaseous phase.

4.3.3.2 Morphological and elemental study

Surface morphology and textural properties of SS and biochar samples were studied with the help of SEM-EDX analysis, to make out the changes that occurred when it was subjected to pyrolysis process. Fig. 4.7 shows the SEM-EDX images of SS and biochar produced at different operating temperatures. It was observed that SS has lignocellulosic structure and interior part is almost filled up. It has a rough and

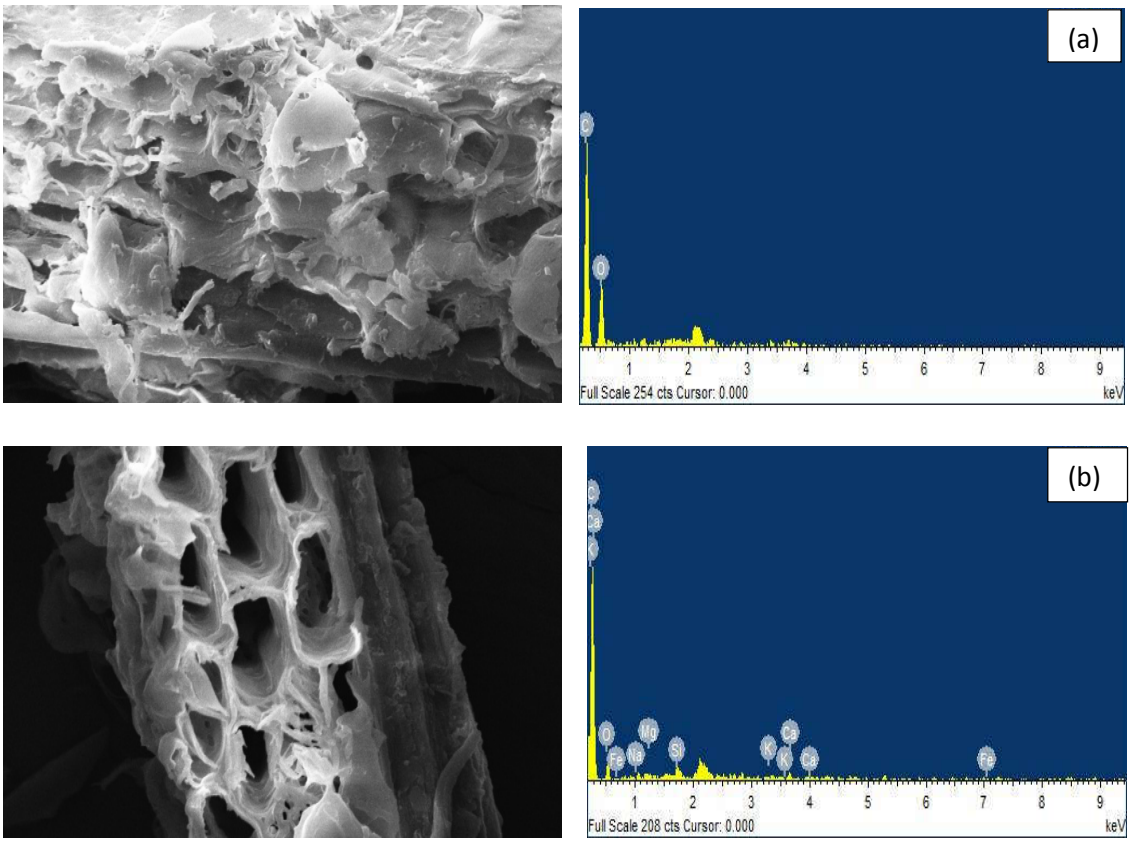

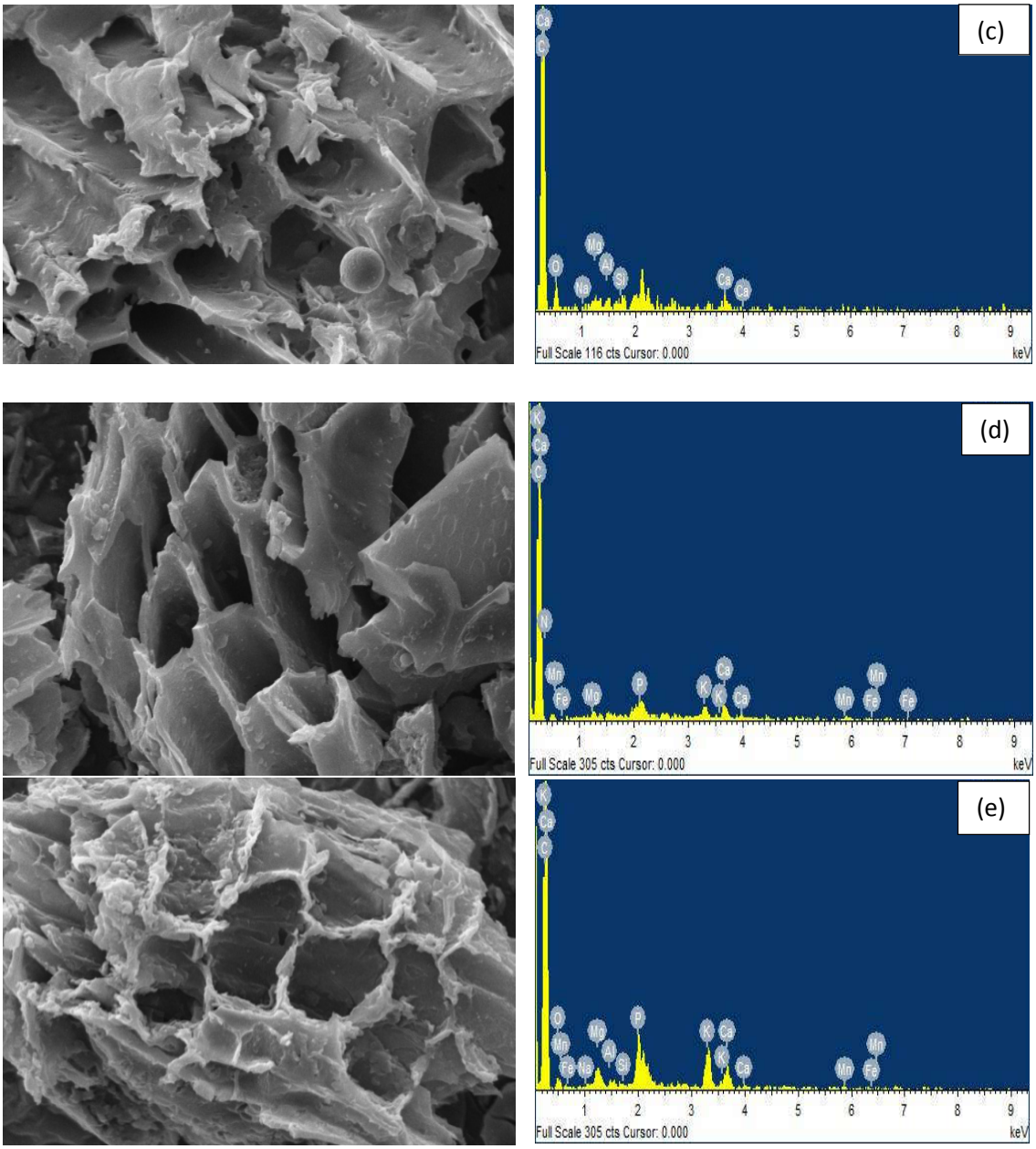

Fig. 4.7 SEM-EDX for (a) SS (b) BC 400 (c) BC 500 (d) BC 600 (e) BC 700

disorganized appearance. Surface of SS is not porous except some cracks and breakages. Structural modifications in biochar samples can easily be compared with precursor image. As and when pyrolysis treatment was applied, volatiles started escaping from the biomass leaving biochar with rough appearance and pores onto the surface which may contribute to more adsorption capacity (Uzun et al., 2010). Honeycomb like structure can be seen in all the biochar samples. The development of

pores in the biochar samples enhanced with increasing temperature, which may result in significant improvement in pore properties of biochar. Highly porous biochars have the advantage of more adsorption sites for metal ions (Rout et al., 2016).

The chemical compositions of the SS and it's biochar were assessed by EDX. The EDX analysis of SS showed that it has mainly C and O in high concentration. After pyrolysis other elements such as Na, Mg, Si, K, Ca, Fe, Mn, P, Al were detected in the biochar samples. These inorganic elements make up the AC of the biochar. With the increase in temperature the concentration of inorganic element was increased and hence AC was also increased.

4.3.3.3 FTIR analysis

FTIR spectroscopy of SS and its biochar produced at different temperatures is shown in Fig. 4.8 to investigate the chemical changes that occurred during pyrolysis. FTIR spectra of biochar differed to a great extent in comparison to SS which could be due to thermal treatment. SS mostly consisted of oxygen-containing functional groups of phenols, alcohols, carboxylic acid and N-H vibrations in the spectral region of 3600–3200 cm^{-1} (Varol and Putun, 2012). These groups were almost invisible in all the biochar samples indicating it was converted to bio-oil products. The peaks of CH_3 and CH_2 (aliphatic C - H band) were present in both SS and biochar samples in the spectral region of 2950–2850 cm^{-1} (Varol and Putun, 2012; Sharma et al., 2004). But these peaks were weaker in biochar samples. This could be because of demethoxylation, demethylation and dehydration of lignin leading to reduction in aliphatic compounds with increasing temperature (Singh et al., 2016). This indicates biochar has become more aromatic and less aliphatic with increase in temperature. The peaks at 1360.2 and 1619.6 cm^{-1} are indicative of lignin in SS (Siengchum et al., 2013; Vincent et al., 2018) whereas peak at 609.6 cm^{-1} represents C-H bending vibration (Angin and Sensoz,

2014). In biochar samples, the broad absorption band from 1700 to 1300 cm^{-1} was associated to C = C skeletal vibration of absorption ring of lignin (Wei et al., 2015). Absorption band from 3100 to 3000 cm^{-1} in biochar samples indicates the presence of C=C-H asymmetric stretch of alkenes and peak in between 900 and 700 cm^{-1} represents C - H out of plane vibration in biochar, which makes it more aromatic carbon (Varol and Putun, 2012).

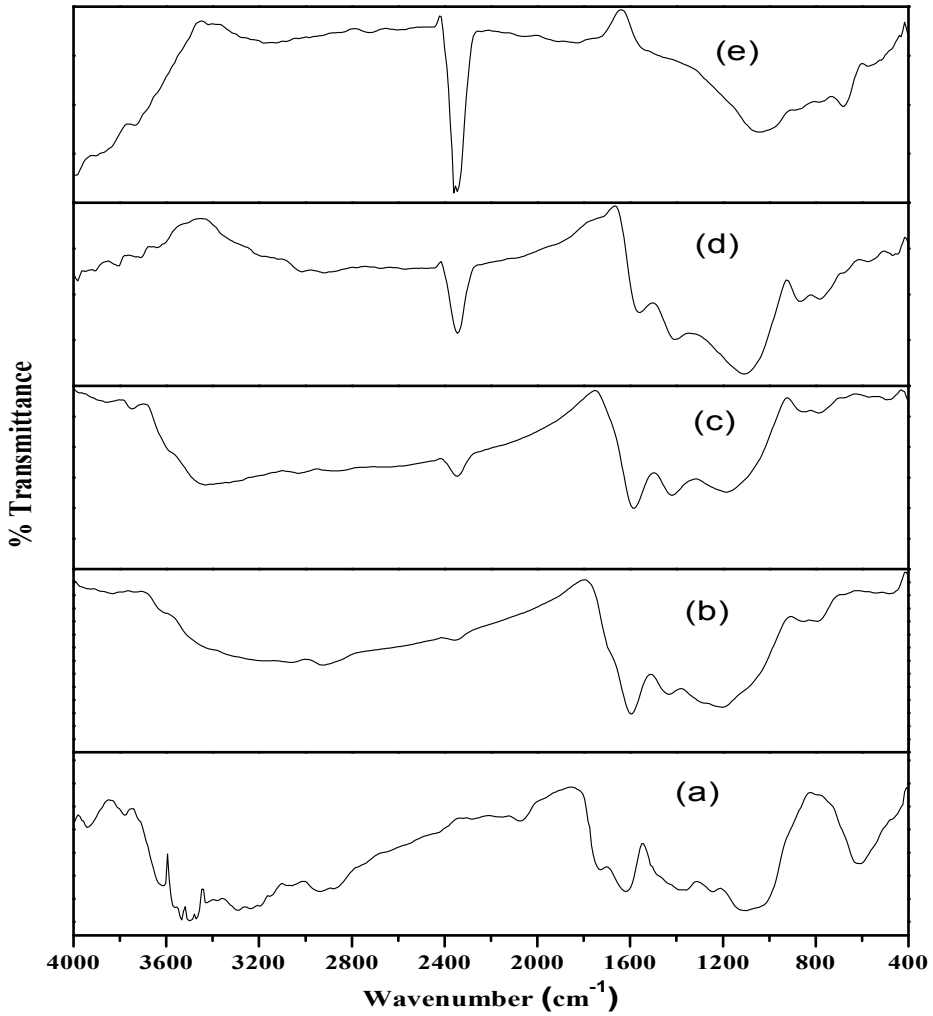

Fig. 4.8 FTIR spectra of (a) SS (b) BC 400 (c) BC 500 (d) BC 600 (e) BC 700

4.3.3.4 BET surface area

BET surface area, pore volume and pore size of biochar are reported in Table 4.2 as it is one of the vital characterizations to study the reactivity and combustion behaviour of biochar. The BET surface area first increased up to 600 ˚C and then it decreased slightly at 700 ˚C but pore volume of biochar increased continuously from 0.002004 to 0.119059 cm^3/g. The BET surface area for BC 400 and BC 500 were less because of the incomplete carbonization and also due to the presence of left over organic matter in it (Chun et al., 2004). However, sudden increase in BET surface area to 253.6631 m^2/g for BC 600 was owing to the release of more amount of VM, creating large number of pores that contributes to its high BET surface area (Shaaban et al., 2013). Similar type of increase in BET surface area was observed by James et al. (2005) for B. pendula wood char where surface area was less than 6.5 m^2/g at temperature below 600 ˚C and it increased to 430 m^2/g at 700 ˚C.

Table 4.2 BET surface area of the biochar at different temperatures

Sample	BET surface area (m^2/g)	Pore volume (cm^3/g)	Average pore size (nm)
BC 400	2.4164	0.002004	35.8891
BC 500	6.8990	0.002338	7.8569
BC 600	253.6631	0.102523	2.9902
BC 700	250.7203	0.119059	2.9216

Pore size of biochar ranged in between 2 and 50 nm which indicates most of the pores are mesoporous according to IUPAC (Singh et al., 2017) and the N_2 adsorption/desorption isotherm for BC 600 is depicted in Fig. 4.9. Increase in pore size

leads to lesser number of micro or meso pores that ultimately give smaller surface area which is confirmed in Table 4.2. Such porous configuration of biochar indicates its enormous adsorption capacity. The increase in surface area with temperature is associated with increase in newly generated meso and micro pores whereas decrease in BET surface area at higher temperature may be due to fusion or merging of smaller pores to larger pores and sintering of smaller pores (Zhai et al., 2017).

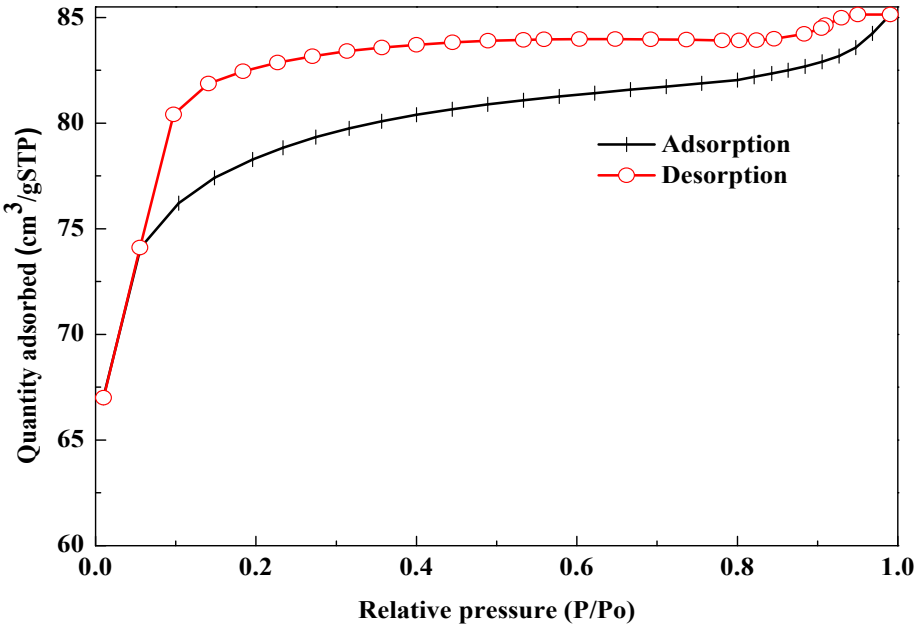

Fig. 4.9 N_2 adsorption/desorption isotherm of SS biochar at 600 °C

4.3.3.5 XRD analysis

The XRD analysis of SS and its biochar is presented in Fig. 4.10. The intensity and sharpness of the peak at 2Θ values around 18° and 22° for SS signifies the presence of amorphous and crystalline cellulose. However, pyrolysis resulted in a complete change of crystallographic nature of biochars in comparison to SS. These peaks got diminished

at higher temperature indicating the degradation of cellulose (Wang et al., 2009). Two peaks were observed in 25–30˚ (2Θ range). One of the peaks at 2Θ ~ 26.6° belongs to the crystallographic structure of quartz. Presence of such peak has been reported by other investigators also (He et al., 2018). The second peak at 2Θ ~ 29.3° corresponds to the crystallographic structure of calcite (He et al., 2018). The increase in the sharpness of the peaks with increase in temperature is attributed to the relative decrease in the amorphous organic phase and increase in the percentage of AC as well

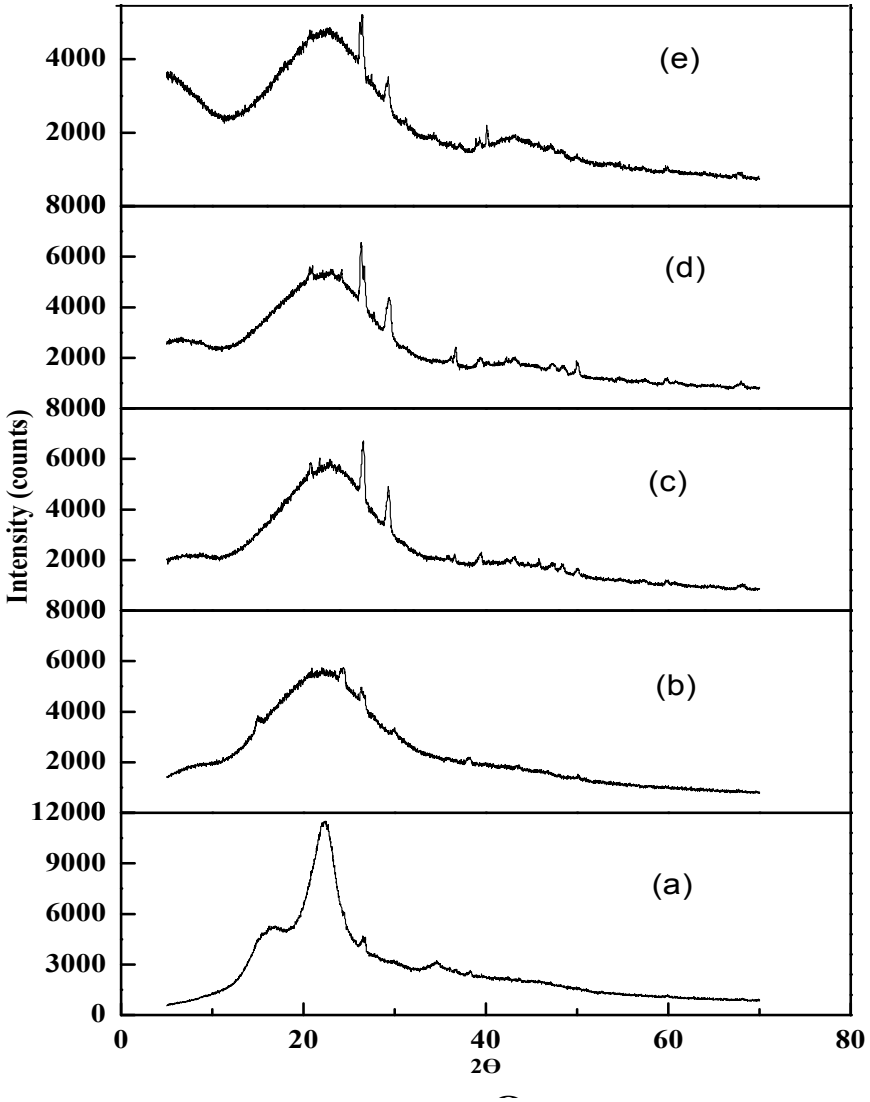

Fig. 4.10 XRD analysis of (a) SS (b) BC 400 (c) BC 500 (d) BC 600 (e) BC 700

as due to the ultrastructural changes in the SS biochar (Zhang et al., 2015; Abrego et al., 2009). Crystallinity index (CrI) calculated from the XRD result is depicted in Table 4.3. A higher value of CrI indicates higher degree of crystallinity and higher amount of cellulose.

Table 4.3 Crystallinity index for SS and biochar at different temperatures

Sample	CrI (%)
SS	57.28
BC 400	22.84
BC 500	22.73
BC 600	22.29
BC 700	20.00

4.3.4 Bio-oil characterization

4.3.4.1Physicochemical properties of bio-oil

Physical properties of bio-oil collected after SS pyrolysis at different temperatures is presented in Table 4.4. The physical appearance of bio-oil was dark brownish in colour having pungent smell. With increase in temperature HHV increased that may be due to lesser amount of oxygenates in sample at higher temperature. The HHV of bio-oil was higher than the HHV of SS but it was lower as compared to available commercial fuels. However, up gradation of bio-oil will enhance the HHV. pH of bio-oil samples were within the range of 2.5–2.9. This is because bio-oil mainly contains organic acids like acetic acid, carboxylic acid which lowers the pH. Kinematic viscosity of the obtained bio-oil at optimum temperature was 28.48 centistokes (cSt) which was lower in

comparison to the bio-oil obtained from rapeseed cake by Ozcimen and Karaosmanoglu (2004). Lower viscosity has the advantage of better flow characteristics. Higher temperature leads to more cracking of biomass components which increases the heavy

Table 4.4 Physicochemical properties of the bio-oil at different temperatures

Property	BO 400	BO 500	BO 600	BO 700
Apperance	Brown	Brown	Brown	Brown
Carbon residue (wt %)	2.31	2.4	2.55	3.38
Ph	2.54	2.45	2.81	2.47
Density (kg/m^3)	1070.1	1082.4	1086.0	1097.8
Viscosity (cSt)	22.47	25.61	28.48	30.84
HHV (MJ/kg)	14.51	17.98	22.19	25.83
AC (wt. %)	0.03	0.04	0.06	0.10

organic fraction and density of the bio-oil. Similarly, the AC for the bio-oil samples were very less and it was in the range of 0.03 – 0.10 wt. %. Carbon residue for all the bio-oil samples were less than 4% and lowest at lower temperature. This may be due to the presence of large amount of lower hydrocarbons at lower temperature. Bio-oil after up gradation can be used for blending with conventional fuels besides the recovery of valuable chemicals (Islam et al., 2008).

4.3.4.2 FTIR analysis of bio-oil

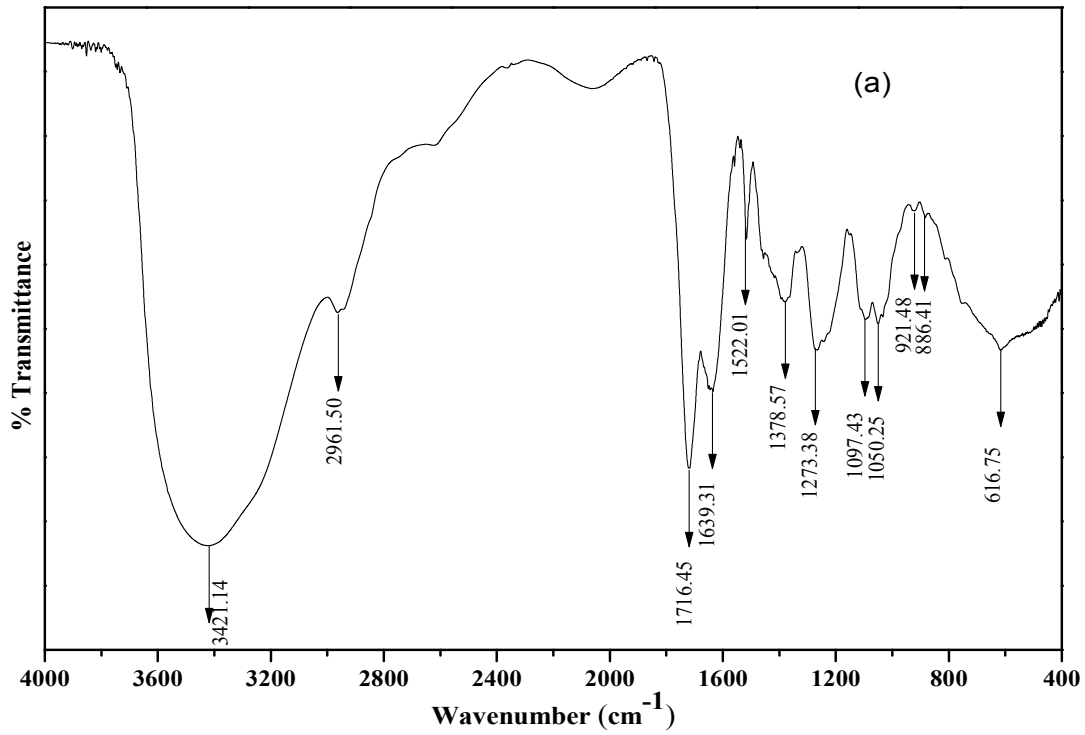

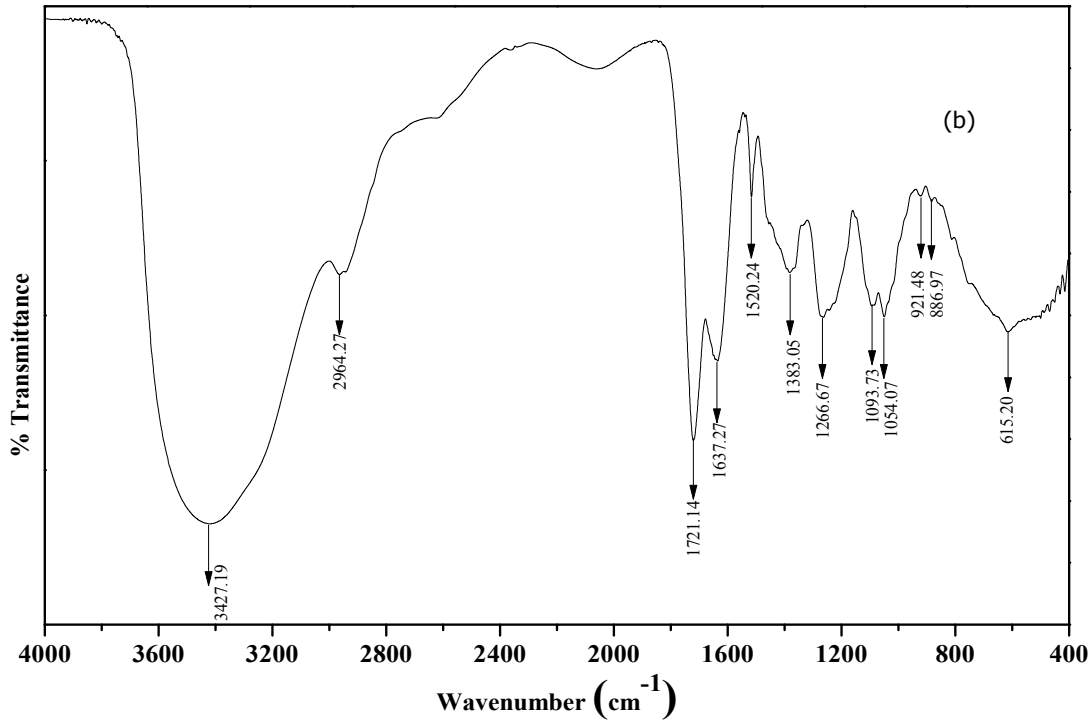

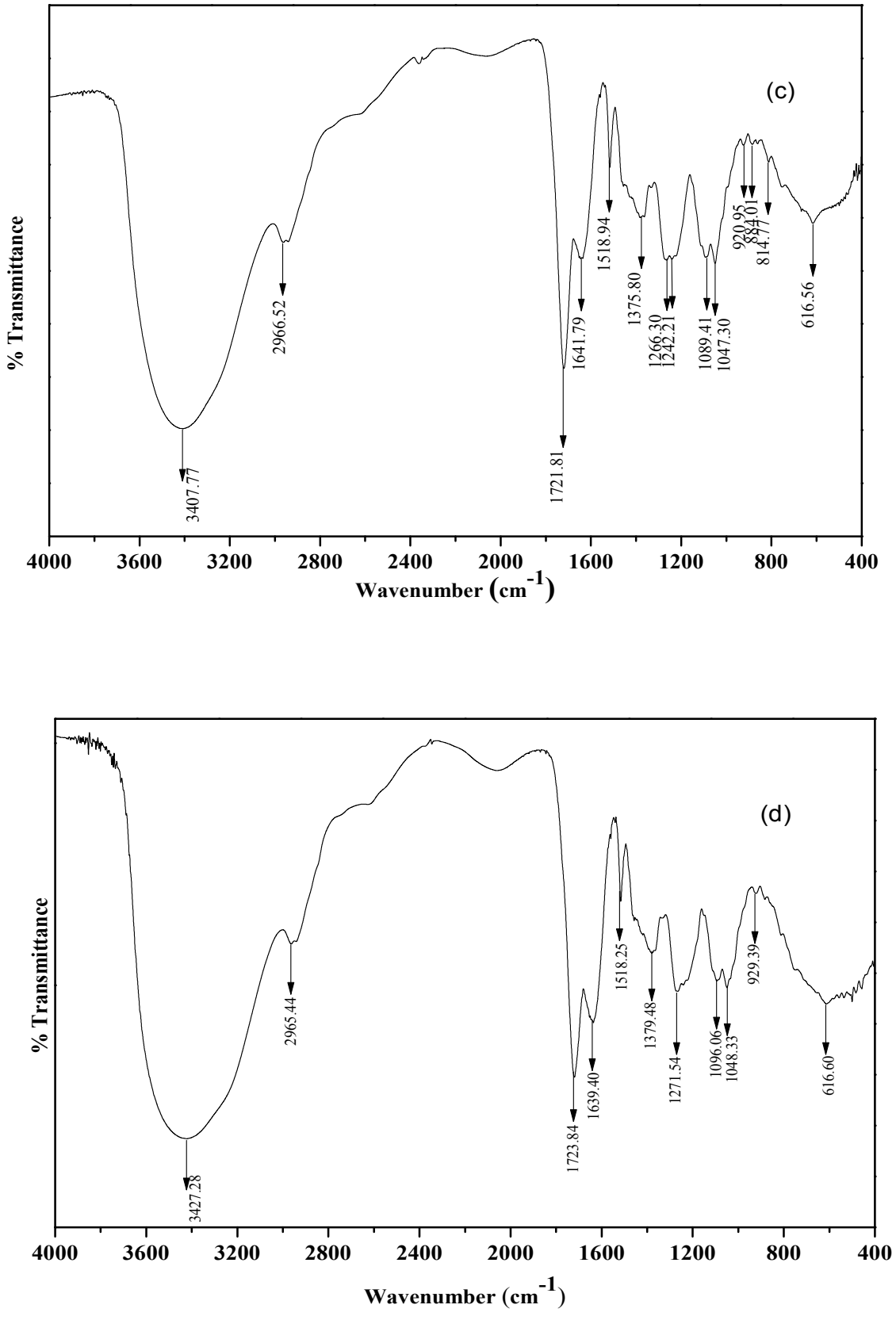

Fig. 4.11 FTIR spectra of bio-oil at (a) 400 °C (b) 500 °C (c) 600 °C (d) 700 °C

FTIR is an important analytical technique for the detection of various functional groups present in bio-oil. FTIR spectra of bio-oil obtained from SS pyrolysis at different temperatures are given in Table 4.5 and Fig. 4.11 (a–d). It is clearly observed from the figure that bio-oil contains large number of atomic groups of which are C-H, O-H, C=O, C=C and C-O. A large broad peak in between 3400 and 3600 cm^{-1} is associated with the O-H group of phenols and alcohols (Rout et al., 2016). Peaks in between 2960 and 2970 cm^{-1} are attributed to C-H stretching of alkanes and alkenes in bio-oil (Capunitan and Capareda, 2012). Two peaks were observed in between 1630 and 1730 cm^{-1} in all the bio-oil samples which indicate C=O stretching vibrations of carbonyl group present in the bio-oil. These stretching vibrations show the presence of aldehydes, ketones and carboxylic acids (Demiral and Kul, 2014). The peaks at 1522, 1520, 1523 and 1518 cm^{-1} correspond to C=C stretches in benzene ring (Karaosmanoglu et al., 1999). Large numbers of peaks in between 1040 and 1280 cm^{-1} are associated with C-O stretch of ethers and esters present in bio-oil (Abnisa et al., 2013; Capunitan and Capareda, 2012). C-H deformations peaks are observed at 1378, 1383, 1375 and 1379 cm^{-1} in all bio-oil samples that indicates the existence of alkane groups (Abnisa et al., 2013). C-H bending vibrations at 880–890 cm^{-1} indicate the presence of vinylidene group in the bio-oil (Gaurh and Pramanik, 2018). Moreover, C-H vibrations of alkene and alkynes were observed in the range of 920–930 cm^{-1} and 610– 620 cm^{-1} (Abnisa et al., 2013). An additional peak of mono and polycyclic aromatic group was observed at 814 cm^{-1} for bio-oil at 600 ˚C (Capunitan and Capareda, 2012). Thus, it can be summarized that bio-oil obtained from SS pyrolysis is a mixture of valuable organic compounds containing paraffin, aromatics etc that can be used as liquid fuel after upgradation or as source of valuable chemicals. However, some of the compounds have similar functional groups

and it does not give a clear idea for identification of particular species. The detailed information about bio-oil was obtained from the GC–MS analysis.

Table 4.5 FTIR peak details of the bio-oil at different temperatures

Wavenumbers (cm^{-1})					
BO 400	**BO 500**	**BO 600**	**BO 700**	**Functional group**	**Probable compound**
3421.14	3427.19	3407.77	3427.28	O-H	Phenols, alcohols
2961.50	2964.27	2966.52	2965.44	C-H	Alkanes/alkenes
1716.45	1721.14	1721.81	1723.84	C=O	Carboxylic acids, ketones, aldehydes
1639.31	1637.27	1641.79	1639.40	C=O	Aldehydes, Ketones
1522.01	1520.24	1523.54	1518.25	C=C	Benzene
1378.57	1383.05	1375.80	1379.48	C-H	Alkane
1273.38	1266.67	1266.30	1271.54	C-O	Ethers and esters
-	-	1237.14	-	C-O	Ethers and esters
1097.43	1093.73	1089.41	1096.06	C-O	Ethers and esters
1050.25	1054.07	1047.30	1048.33	C-O	Ethers and esters
921.48	921.48	920.95	929.39	C-H	Alkenes
886.41	886.97	884.01	-	$C=CH_2$	Vinylidene group
-	-	814.77	-	C-H	Aromatics
616.75	615.20	613.82	616.60	C-H	Alkynes

4.3.4.3 GC–MS analysis of bio-oil

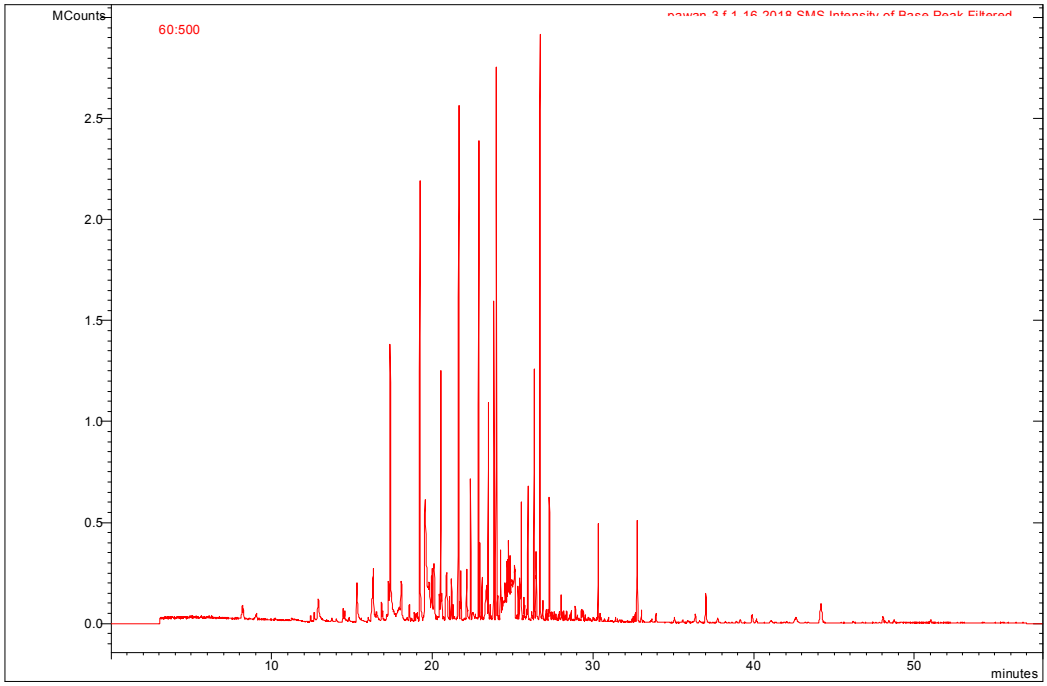

Fig. 4.12 GC-MS analysis of bio-oil at 600 °C

The complex chemical composition of bio-oil was further analyzed using GC–MS technique to get the idea of the probable compounds formed after pyrolysis of SS as shown in Fig. 4.12. The chromatograph peaks and list of probable compounds formed along with retention time (RT) and area % are depicted in Table 4.6. The compounds generated in the bio-oil were formed mostly due the thermal degradation of biomass components i.e. hemicelluloses, cellulose and lignin. In general, bio-oil is a mixture of branched/stretched chain organic compounds mainly aliphatics, aromatics, aldehydes, ketones, mixed acids, esters and phenols according to the results of FTIR analysis (Saikia et al., 2015). Aldehydes, ketones, carboxylic acids and esters are the main oxygenated group of compounds present in the bio-oil. These oxygenated compounds such as 2- heptanone, acetic acid-decyl ester, etc. are formed after the decomposition of

cellulose and hemicellulose portion of biomass (Yorgun and Yildiz, 2015). Lignin portion of biomass was responsible for the generation of phenol content and its derivatives such as: phenol, 2- allyl-3, 4 dimethoxy phenol, 2-methoxy 4-propyl phenol (Yorgun and Yildiz, 2015). Among the identified compounds, a major portion contributes to phenols and its derivatives in agreement with the results of other researchers as well. Higher amount of phenols and its derivatives also contributes to the higher HHV of the bio-oil (Nanda et al., 2014). Further upgradation of bio-oil can enhance the calorific value and thereby corrosiveness of the fuel can be reduced after separating the oxygenated compounds. Biooil can also be considered as valuable source of chemicals such as phenols which is considered as one of the important commercial compound (Jiang et al., 2014).

Table 4.6 GC-MS analysis of bio-oil at 600 °C

Sl. No.	Retention time (RT)	Compound	Molecular formula	Area (%)
1	8.184	1-Methyl-2 cylopenten-1 ol	$C_6H_{10}O$	1.378
2	13.018	2- Heptanone	$C_7H_{14}O$	0.242
3	15.297	Phenol	C_6H_6O	5.969
4	16.845	4- Formylfuran-2(5H)-one	$C_5H_6O_3$	8.600
5	17.378	Alpha-hydroxy-p-cresol	$C_7H_8O_2$	5.629
6	19.222	2 Methoxy-4 methyl phenol	$C_8H_{10}O_2$	4.281
7	19.544	Acetic acid, decyl ester	$C_{12}H_{24}O_2$	12.473
8	20.528	2,5Dimethoxytoluene	$C_9H_{12}O_2$	0.549
9	21.654	Napthalene, 2-ethenyl	$C_{12}H_{10}$	2.802

10	21.785	2,6-Dimethoxy phenyl propyl ester	$C_{17}H_{24}O_6$	8.184
11	22.384	3-Hydroxydeconic acid	$C_{10}H_{20}O_3$	1.221
12	22.883	4-Hydroxy-3-methoxy benzoic acid	$C_8H_8O_4$	3.731
13	22.955	Isoeugenol (II)	$C_{10}H_{12}O_2$	4.695
14	23.485	1-Ethynyl-3 methyl napthalene	$C_{13}H_{10}$	10.545
15	23.834	5-tert-Butyl pyrogallol	$C_{10}H_{14}O_3$	1.252
16	23.986	cis-Corniferyl alcohol	$C_{10}H_{12}O_3$	1.010
17	24.638	2 Propenoic acid, 3-(4-hydroxy-3-methoxy Phenyl)	$C_{10}H_{10}O_4$	0.697
18	24.752	Phenol,2-6-dimethoxy-4 propenyl	$C_{11}H_{14}O_3$	0.359
19	25.541	3H-4 Naptho[3,4-b] pyran	$C_{13}H_{10}O$	1.702
20	25.946	2-Allyl-3,4 dimethoxy phenol	$C_{11}H_{14}O_3$	1.849
21	26.340	2 Methoxy-4 propyl phenol	$C_{10}H_{14}O_2$,	4.658
22	26.702	1-1-Diphenyl-2 methyl propane	$C_{16}H_{18}$	11.073
23	27.287	4 Phenyl propiophenone	$C_{15}H_{14}O$	2.872
24	30.324	7-Methyl-9,10-anthraquinone 1-carboxylic acid	$C_{16}H_{10}O_4$	1.650
25	32.751	2,3-bis (4-hydroxy-3 methoxy benzyl)-1,4-butanediol	$C_{20}H_{26}O_6$	2.580
26	37.026	4-[2-(4-Allyl-2-6 dimethoxy phenoxy)-1-hydroxy] 2-6-dimethoxy phenol	$C_{22}H_{28}O_7$	0.367

4.3.5 Pyrolytic gas composition

The variations in pyrolytic gas composition from SS pyrolysis at different temperatures were studied using GC-TCD and GC-FID as shown in Fig. 4.13 (a). The concentrations of the pyrolytic gas samples were calculated using the calibration curves prepared from known concentrations of the pure gases. It was observed that pyrolytic gas produced mainly consist of hydrogen (H_2), methane (CH_4), carbon monoxide (CO) and carbon dioxide (CO_2). So, GC-TCD was used for the detection of H_2 whereas GC-FID was used for the detection of CO, CO_2 and CH_4, respectively.

CO and CO_2 were the dominant gases at lower temperature i.e. at 400 ˚C. The release of CO and CO_2 occurs due to the degradation of hemicellulose and cellulose (Dhyani and Bhaskar, 2018) because both these components degrade at the temperature of around 400 ˚C. The release of CO_2 was due to the cracking and reforming of C=O and COOH functional groups present in SS (Jahirul et al., 2012). However, release of CO_2 at higher temperature was because of lignin degradation. The concentration of CO decreased from 21.23 mol % at 400 ˚C to 9.31 mol % with increase in pyrolysis temperature. The release of CO was due to cracking of carbonyl (C-O-C) and carboxyl (C=O) groups present at lower temperatures (≤ 600 ˚C) and at higher temperature; its release was due to small amount of cellulose and lignin decomposition. The release of CO and CO_2 also specify the presence of oxygen in SS as pyrolysis experiments were performed in inert atmosphere. Thus, cellulose and hemicellulose are mostly responsible for the release of CO and CO_2. The evolution of methane (CH_4) from the pyrolysis of SS was associated with the cracking of methoxy (O-CH3) group. The concentration of methane was lower (1.65 mol %) at 400 ˚C but it reached to a maximum (10.89 mol %) at 600 ˚C and then it decreased. All the three components of SS contribute to methane release in their degradation temperature range but it was highest due to the

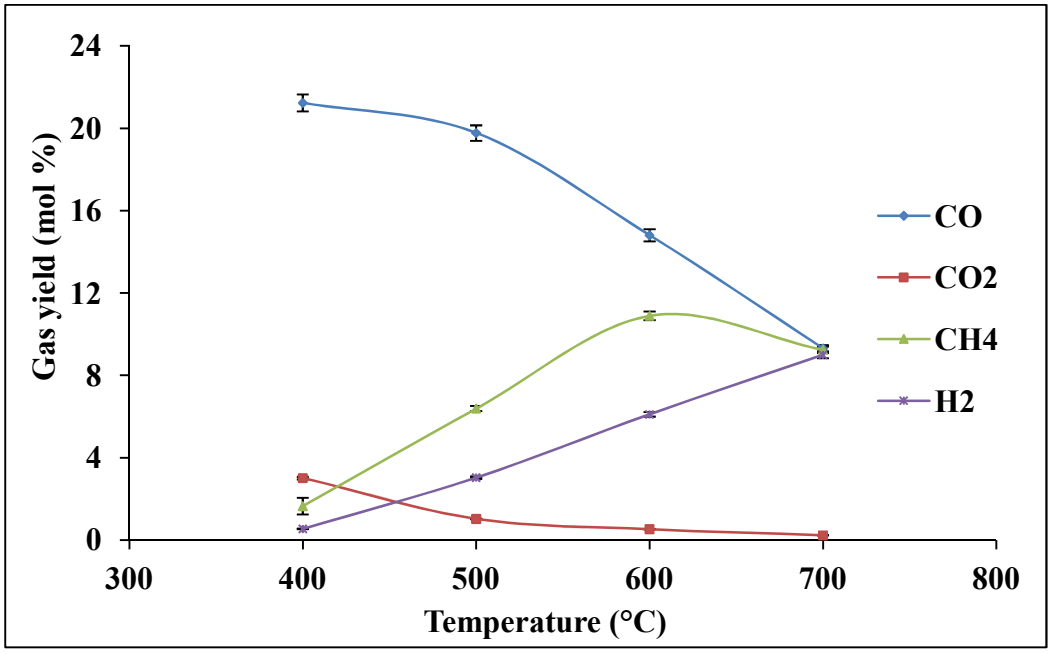

(a)

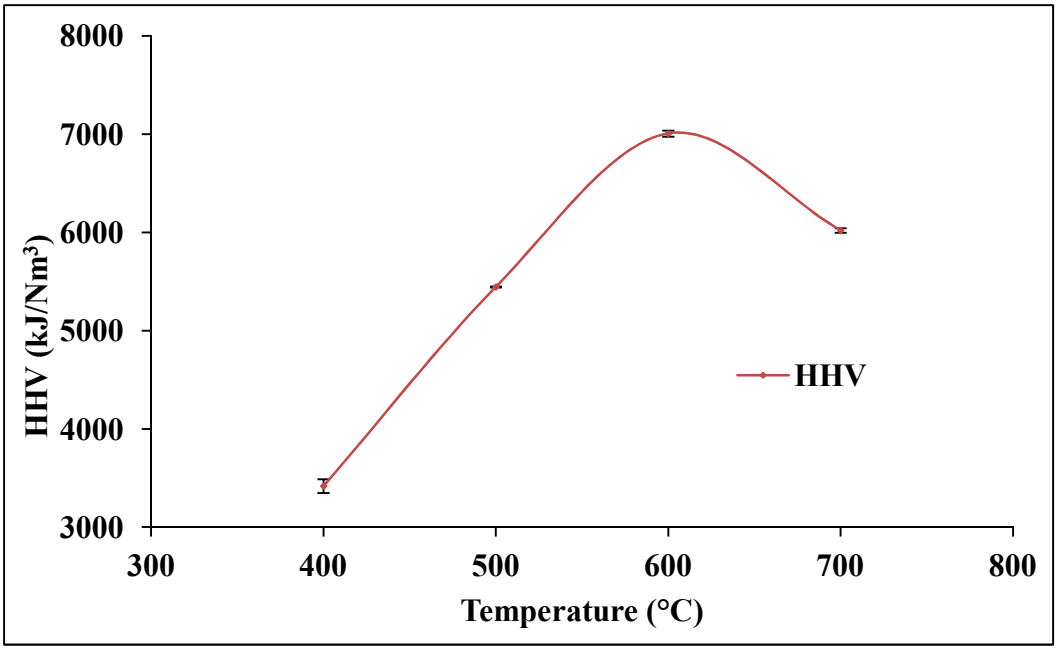

(b)

Fig. 4.13 Non-condensable gas fraction (a) composition (N_2 involved) (b) HHV at different pyrolysis temperature

degradation of lignin as it has highest O-CH3 content (Yang et al., 2007). On the other hand hydrogen concentration was increasing with temperature and it was maximum (8.99 mol %) at 700 ˚C. The release of hydrogen was mainly due to cracking and decomposition of aromatic rings and methoxy groups of lignin. The study of HHV of pyrolytic gas is important as it describes its potential to be used as fuel. The presence of methane and hydrogen in the gas composition provides good fuel properties and can be used for the generation of energy. The HHV of pyrolytic gases at various temperatures were calculated using equation as given by Guangul et al. (2014) and it is depicted in Fig. 4.13 (b). The maximum HHV of pyrolytic gas calculated was 7006.67 kJ/Nm^3 at 600 ˚C. The decrease in HHV at higher temperature was due to lesser production of methane. The pyrolytic gas can be combusted to provide process heat to different operations. Also, it can be recycled to enhance the bio-oil yield and its properties (Mante et al., 2012; Dhyani and Bhaskar, 2018).

4.4 Conclusion

The pyrolysis experiments with SS were performed in a packed bed reactor in inert atmosphere. The yields of biochar, bio-oil and pyrolytic gas from SS pyrolysis were found to be 27.4, 48.8 and 23.8%, respectively at temperature of 600 C, N_2 flow rate 150 mL/min, packed bed height 8 cm and particle size of 0.18–0.25 mm. The bio-oil yield was in the range of 42.24 to 48.80% and the temperature for maximum bio-oil yield was 600 ˚C. HHV of bio-oil varied from 14.51 to 25.83 MJ/kg. Obtained bio-oil was a mixture of aliphatic, aromatic and oxygenated hydrocarbon as confirmed by FTIR and GC–MS. Bio-oil can be used as synthetic liquid fuel or as feedstock for valuable chemicals. Biochar yield was decreasing with increase in temperature. SEM and BET analysis confirmed its porous nature that can be used as adsorbent in waste water treatment. The HHV of biochar increased sharply in comparison to SS and had high

BET surface area of 253.6631 m^2/g. HHV of biochar was also high and was in the range of coal found in India. Pyrolytic gas had good proportional of H_2, CH_4, CO and CO_2 in exit gas stream. These gases after cleaning can be used as feedstock in Fischer-Tropsh process for production of mixture of liquid hydrocarbons. Therefore, pyrolysis of SS for the production of valuable products can be effective in waste minimization, waste treatment as well as in energy generation.

Following this, statistical optimization using RSM was executed to get the optimized process conditions for SS pyrolysis as discussed in chapter 5.